Phys. Status Solidi RRL **10**, No. 3, 242–247 (2016) / **DOI** 10.1002/pssr.201510433

pss +++rapid research letters+++
www.pss-rapid.com

Magnetoelectric oxide films for spin manipulation in graphene

S. C. Stuart[**,1], **B. Gray**[1], **D. Nevola**[1], **L. Su**[1], **E. Sachet**[2], **M. Ulrich**[1,3], **and D. B. Dougherty**[*,1]

[1] Department of Physics, North Carolina State University, Raleigh, NC 27695, USA
[2] Department of Materials Science and Engineering, North Carolina State University, Raleigh, NC 27695, USA
[3] Army Research Office, Durham, NC 27703, USA

Received 25 November 2015, revised 8 January 2016, accepted 18 January 2016
Published online 28 January 2016

Keywords magnetoelectrics, spintronics, Cr_2O_3, films, graphene, spin field effect transistors, scanned probe microscopy

[*] Corresponding author: e-mail dbdoughe@ncsu.edu
[**] Present address: Microelectronic Technology Department, The Aerospace Corporation, Los Angeles, CA 90009-2957, USA

The challenge of creating a graphene spin field effect transistor (spin-FET) demands a magnetic gate dielectric material whose magnetization can be switched electrically. We have grown films of Cr_2O_3 on top of graphite and graphene by pulsed laser deposition that shows this crucial functionality. We demonstrate that the Cr_2O_3 films are magnetoelectric by poling them in combined electric and magnetic fields and then using magnetic force microscopy to observe spontaneous surface domain structure as a function of poling field. In addition, we show that the electric field created by a conducting AFM tip can be used to write magnetic patterns in the film that demonstrate the kind of continuous magnetoelectric control needed for a prototype spin-FET.

1 Introduction Graphene is an exciting new material for spin-electronics, or "spintronics", because it can combine high carrier mobility with long spin lifetime to efficiently transport spin polarized currents over large distances [1]. While there remain challenges surrounding maximizing and understanding the spin lifetime in graphene, it is already on par (100 ps–1 ns) [1] with single crystal-silicon [2] as among the highest known, especially at ambient temperatures. It is timely to press forward with the next essential step in spintronic device technology: *spin manipulation*. We need to find ways to control the spin information in an ensemble of carriers to identify new approaches to information processing.

The classic device architecture for manipulation of spin polarized carriers is the spin field effect transistor (spin-FET) where magnetic interactions with a gate control spin precession in a conducting channel. Datta and Das proposed the first spin-FET based on the mechanism of electric field-controlled Rashba spin–orbit coupling at an interface between a gate and a conducting channel [3]. However, in graphene long spin lifetimes arise precisely because spin–orbit coupling effects are small in carbon. In the case of graphene, we need to search for an alternate *mechanism* of spin manipulation in a spin-FET. Possibilities include the use of magnetic adsorbates or substitutional dopants [1] to control magnetic scattering in graphene. More recently, the rise of new 2D layered materials has led to attempts to imprint spin–orbit interactions in graphene by proximity to a stronger spin–orbit material [4]. Another option is to use exchange interactions with a magnetic gate material in close proximity to the graphene. This is the basis for our exploration.

Several theoretical proposals exist for spin manipulation in graphene by direct exchange interactions with a magnetic gate [5, 6]. But what specific material should be used and what is the mechanism of gate-bias controlled exchange interactions? To address these important questions, we need to integrate multifunctional materials that allow electrical control of interfacial magnetism. Magnetoelectric oxides [7] are a simple approach to creating the *electrically-controlled* exchange interactions needed for a graphene spin-FET and were mentioned in the initial proposal by Semenov et al. [6]. In addition, a recent U.S. patent has been issued including this idea [8]. In this communication, we provide experimental evidence for the magnetoelectric functionality of oxide films on graphite and graphene substrates that is needed for eventual use in prototype spin-FETs.

Our premier magnetoelectric candidate oxide is Cr_2O_3. This material has a linear magnetoelectric coefficient that leads to a linear dependence of bulk magnetization on applied *electrostatic* field [7, 9]. Furthermore, it has been shown that the magnetoelectric functionality at the surface of a film can be relatively insensitive to surface roughness [10]. Thus, even though graphitic substrates are challenging for oxide growth, there is hope of maintaining key properties of a Cr_2O_3 gate. Importantly, recent work [10–17] has shown a unique surface (or interface) magnetization for Cr_2O_3 that will be crucial to overcome the intrinsically small bulk magnetoelectric coefficient [7].

We take the view that spin-FETs using magnetoelectric oxide gates will benefit from gate deposition directly on top of graphene as opposed to transfer of graphene to a preexisting gate oxide. This is because optimization of spin lifetime in graphene is nontrivial and can be degraded by structural defects and impurity scattering that can arise in the transfer process [1]. It will be advantageous to create the very highest quality graphene substrate for spin transport and then perform controlled magnetoelectric top-gate growth. Remarkably, high-quality crystalline EuO growth on top graphene has been demonstrated using oxide molecular beam epitaxy even though lattice and symmetry matching at the interface is not ideal [18]. Along with other reports of Cr_2O_3 growth on graphitic carbon [19], this indicates a very promising future for functional oxide film growth on graphene.

2 Experimental Films of Cr_2O_3 were deposited on HOPG and on single layer graphene on SiC(0001) by PLD in a turbo-pumped chamber with a base pressure of 5×10^{-7} Torr. The films were grown by ablating a chromium oxide target (Cr_2O_3, Kurt J. Lesker, 99.995%) in an oxygen atmosphere of either 10 mTorr or 100 mTorr using a Light-Machinery Pulsemaster model 860 excimer laser. The laser was used with a standard KrF gas mixture to obtain a 248 nm wavelength at a fluence of ~2 J/cm^2 with 150 mJ of power at the target with a 50 Hz repetition rate. Substrate temperature was typically held at approximately 400 °C using a quartz lamp heater monitored by a thermocouple placed near the substrates. Film thickness was calibrated using XPS measurements of the ratio of intensities C1s/Cr2p$_{3/2}$ (see Supporting Information, Fig. S5) HOPG substrates were cleaved with adhesive tape before loading into the PLD chamber. Graphene on the Si face of SiC was grown as described previously [20]. XPS measurements showed dramatically reduced sticking coefficients for Cr_2O_3 on graphene/SiC compared to HOPG. This did not affect the magnetoelectric functionality observed by MFM/EFM.

An Asylum MFP-3D AFM was used to measure the Cr_2O_3 film topography and magnetoelectric properties using EFM, MFM, and magnetoelectric writing at room temperature in ambient air. Tips for AFM imaging (Budget Sensors Tap300-Al-G, ~40 N/m), magnetoelectric writing (Budget SensorsElectriCont-G, ~0.2 N/m), and EFM (Budget Sensors ElectriTap300-G, ~40 N/m) were used as received. Tips for MFM (Budget Sensors MagneticMulti75-G, ~3 N/m) were brought in proximity (less than ~1 cm) to a permanent magnet prior to imaging. Films were magnetoelectrically annealed in ambient air by placing the sample on a grounded niobium permanent magnet located ~1 cm below a thin (~0.2 mm) steel plate. The plate was held at a potential difference of 1–3 kV with respect to the grounded magnet to form a parallel plate capacitor annealing stage. The magnetic field near the surface of the permanent magnet where the sample is mounted during magnetoelectric annealing was measured to be ~1 T with a Hall effect Gaussmeter.

X-ray diffraction (XRD) was measured using a PANayltical Empyrean diffractometer with a Cu K_α source ($\lambda \approx 1.54$ Å), a programmable divergence slit, and an X'Celerator detector in the θ–2θ mode. XPS for thickness calibration was carried out using a Riber instrument with base pressure 2×10^{-10} Torr, a MAC-2 electron detector, and a Mg K_α source (1247 eV). XPS for detailed analysis of the C 1s line shape and the Cr 2p line shape was carried out using a Specs hemispherical analyzer (Phoibos 150) in normal emission with a Mg K_α source. In-situ annealing to

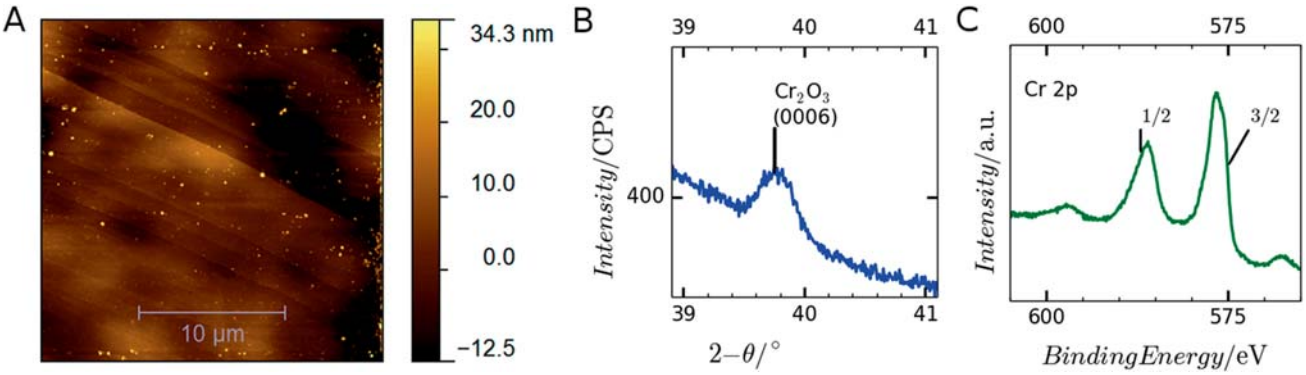

Figure 1 Structural and chemical properties of a 40 ± 10 nm Cr_2O_3 film grown on HOPG. (A) Topography of a chromium-oxide film grown on HOPG with major features representative of the HOPG surface, and some particulates common to the PLD process. (B) A Cr_2O_3(0006) peak with a FWHM of 0.32° for a film grown at 400 °C. (C) Cr 2p XPS with a structure characteristic of Cr_2O_3.

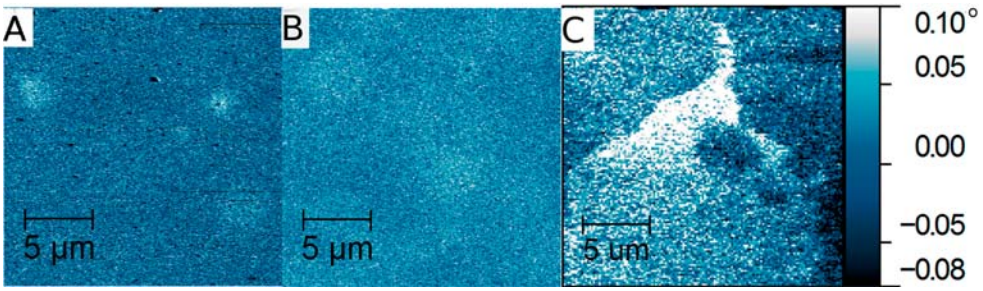

Figure 2 Magnetic domains produced in the film in Fig. 1 by magnetoelectric annealing in ~1 T applied magnetic field and variable electric fields. (A) Small domains (~2 μm) produced by a 1.75 kV/cm electric field; (B) larger domains (~5 μm) produced by 1.875 kV/cm electric field. (C) A much larger (~15 μm) domain produced by a 2 kV/cm field. Scale bar applies to all images.

remove physisorbed contaminants was conducted using a commercial UHV heater with line of sight to the back of the sample after samples were transferred in air to the XPS chamber. The XPS binding energy scale was calibrated by assigning the C 1s main line to be 284.5 eV.

3 Results We have used pulsed layer deposition (PLD) to grow Cr_2O_3 films of variable thickness on top of graphene on SiC and graphite. In Fig. 1A, we show an atomic force microscope (AFM) image of one such film grown on highly-oriented pyrolytic graphite (HOPG) with a thickness of 40 ± 10 nm. The overall smooth morphology (roughness 6.7 nm RMS with particulates included, 2.2 nm RMS without) exhibits linear defects arising from substrate step bunches and some particulates from the PLD growth process. X-ray diffraction in θ–2θ mode in Fig. 1b shows a weak (0006) peak at 39.8° corresponding to *c*-axis texture along the substrate surface normal. X-ray photoelectron spectra such as shown in Fig. 1c exhibit Cr $2p_{3/2}$ core level peaks with a shoulder-like structure on the low binding energy side that is a fingerprint of Cr_2O_3 [21].

Figure 2 shows magnetic force microscopy (MFM) images of the effect of magnetoelectric poling of the 40 ± 10 nm Cr_2O_3 film on graphite subjected to both a ~1 T magnetic field perpendicular to the surface and different applied electrostatic biases. Single magnetic domains are achieved for ~3 kV/cm (not shown since a single domain has no spatial contrast). At lower magnetoelectric annealing biases of 1.75, 1.85 and 2 kV/cm (as shown in Fig. 2A, B and C, respectively) magnetic domains can be seen as lighter blue regions whose average size increases with increasing bias. This is intuitively plausible since the purpose of the combined fields is to pole a single domain and if this will be less effective for weak fields. More

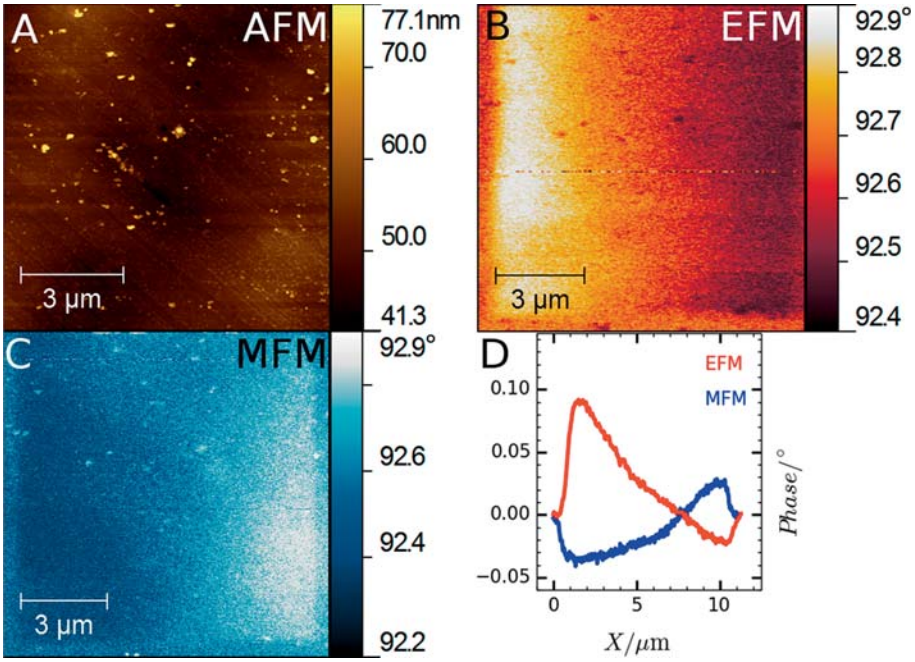

Figure 3 Results of applying a local electric field varying from 2.5 V to –2.5 V with a conducting AFM tip in contact with the surface. (A) Topography; (B) EFM; (C) MFM; (D) averaged horizontal line profiles over the entire pattern from the magnetization and polarization in Fig. 3B and C.

quantitatively, it is likely to be connected to the observations of other groups [10, 15] that magnetoelectric annealing switches exchange bias sign under conditions of applied electric and magnetic fields such that the product of the two field strengths is constant. This is broadly consistent with Fig. 2, where only a narrow range of voltages results in significant surface magnetization for a constant applied magnetic field of ~1 T.

Figure 3 shows the important new phenomenon of magnetoelectric writing with a biased AFM tip.We developed this process to more controllably demonstrate the magnetoelectric functionality of our films. A film that is initially poled to be single domain using a large applied electric field can have its local magnetization switched by application of a second local electrostatic field. The local electrostatic field is applied with a biased conducting AFM tip in direct contact with the sample. This electrostatic writing procedure results in both a local electric polarization and a local magnetization. The coexisting functional effects are shown in Fig. 3A, B and C. This figure shows the same area of the Cr_2O_3 film scanned by AFM (shown in gold), electrostatic force microscopy (EFM, shown in red) and MFM (shown in blue). A linear ramp from +2.5 to –2.5 V was written across the surface from left to right, producing a gradient from left to right in the EFM *and* MFM signal. Line profiles averaged over the entire patterned area of the MFM and EFM images are shown in Fig. 3D and show the important capability of continuous oxide gate magnetization and polarization control using an applied bias. The contrast of the MFM and EFM in Fig. 3D is reversed due to the field directions during magnetoelectric annealing and the poling direction of the MFM tip.

4 Discussion Since ordered domains in a magnetoelectric have coupled magnetization and electric polarization, it is important to consider how to reveal both types of order within a single domain. MFM contrast must in principle always contain both electrostatic and magnetostatic contributions. We are able to show that our MFM contrast contains magnetic contributions in addition to electrostatic contributions by two separate control experiments. First, we can distinguish long range forces due to electric charge and magnetization by comparing the bias dependence of contrast in MFM and EFM images (see Supporting Information, Fig. S1). Variable-bias MFM shows that the phase contrast does not invert when we invert the tip-sample bias whereas the phase contrast for EFM does invert with bias. The total phase signal observed is a function of capacitive effects, electrostatic charge, and magnetic interactions [22]. It is clear from contrast reversal with bias that the EFM image is dominated by electrostatic charge effects. Capacitive effects have a quadratic dependence on bias and appear in our EFM measurements as a background level with this quadratic dependence. In MFM, the contrast of written domains does *not* reverse with bias (though capacitive background signal is still present) and is consistent with phase shifts dominated by local magnetization. Further evidence for magnetostatic effects in our MFM measurements comes from a control experiment where we reversed the magnetization of our MFM tip with an ex-situ permanent magnet. As shown in Fig. S2 of the Supporting Information, the result is only a temporary reversal of MFM contrast. After scanning only part of the previously written pattern, the contrast returns to the original sign. This is the result of the stray field from magnetic domain reorienting the tip magnetization. Thus, Fig. 3 combined with control experiments shown in Figs. S1and S2 shows that the Cr_2O_3 films we have grown on graphite are magnetoelectric and can be magnetically controlled by an electrostatic gate.

An additional issue with contact mode writing processes is the question of whether electrochemical processes occur during the writing, such as found in the influential work on complex oxide heterostructures [23]. This is would most likely result in topographic changes in the area where the pattern is written. By inpection of Fig. 3a, which is the topographic image corresponding to the EFM and MFM in Fig. 3b and c, respectively, it is clear that the square pattern does not appear in topography. In the course of numerous writing experiments, we occasionally observed small topographic changes such as changes in position of random particles or slightly modified roughness in the patterned region. While we cannot completely rule out electrochemical effects during our writing process, we do point out the very important fact that the magnetoelectric writing procedure *does not work* if the sample has not been poled in combined electric and magnetic fields. This shows that the writing procedure is intimately connected to the magnetoelectric functionality of the film surface regardless of whether electrochemical processes occur or not.

Magnetoelectric writing of gradients and arbitrary patterns has been repeated for Cr_2O_3 films grown on graphene on SiC(0001) and is shown in Fig. S3 of the Supporting Information. This supports the common intuitive notion that graphite is a good proxy substrate for graphene for the purpose of characterizing new films and interfaces.

The magnetoelectric properties of Cr_2O_3 are anisotropic and the strongest coupling between the electric field and the magnetization (with a proportionality given by the linear magnetoelectric coefficient α) occurs along the *c*-axis of the corundum crystal structure. Therefore it is important to consider the crystal texture of device-relevant films to maximize magnetoelectricity. We find the best combination of crystal orientation and film smoothness is obtained with a growth temperature of 400 °C. The *c*-axis growth texture is not surprising given the matching hexagonal structure of the Cr_2O_3 and HOPG. However the small film roughness (6 nm typical over 20 μm regions) and overall conformity to the substrate is remarkable. In addition, the low intensity of the (0006) diffraction peak suggests that the crystal texture is weak and films are poorly-ordered overall. It important to realize that this means the magnetoelectric functionality of Cr_2O_3 gates on graphitic substrates is forgiving of sub-optimal film crystallography. This is consistent with the roughness inde-

pendence of exchange bias already reported for Cr_2O_3 and is an added advantage of magnetoelectric gates for graphene spin FETs.

To assess the buried Cr_2O_3/graphite interface, a partial coverage film of Cr_2O_3 was deposited on graphite using identical conditions to the thicker magnetoelectric films already described. Most importantly, there is no change in C1s XPS lineshape that would indicate new carbide or carbon-oxygen bond formation after the growth of Cr_2O_3 (see Supporting Information, Fig. S4). In fact, we observe a small *reduction* of relative intensity of a trace carbon–oxygen (e.g. C=O and/or O–C=O) component of the lineshape at ~288 eV [24] after oxide growth when compared to the starting graphite substrate. Due to the evident lack of significant chemical changes at the interface, we infer that graphene is not disrupted by Cr_2O_3 deposited in this fashion and that the dominant effect of the oxide will arise from magnetic exchange. Furthermore, any large scale chemical etching during growth or annealing would appear in the topographic AFM images. We have observed significant etching when some samples were annealed at temperatures above 800 °C. However, large-scale morphological changes were not observed for films grown at 400 °C which show the desired magnetoelectric properties.

Based on this relatively inert interface in combination with the clear magnetoelectric response of thicker films, we consider Cr_2O_3 on graphene to be ideal for proof-of-principle spin manipulation. We do not have direct information on the size of the exchange interactions at the interface and we expect that only dedicated device studies will start to reveal this microscopic detail. However, we can turn to computational studies of related oxide/graphene interfaces to estimate the strength of the exchange effects which can be expected. Haugen et al. estimated ~5 meV exchange interactions for EuO/graphene by analogy with EuO/Al interfaces [5]. Recently, first principles calculations of the EuO/graphene interface have suggested an even larger value of 36 meV for the proximity-induced exchange gap [25].

Importantly, the unique magnetized surface state of Cr_2O_3 has been observed to result in extraordinary control of exchange bias when in contact with a magnetic CoPt film [10]. In our measurements the uniqueness of the surface is reflected in the remnant magnetic ordering due to magnetoelectric annealing that is different than the bulk. Thus, the surface magnetization of Cr_2O_3 may significantly exceed expectations based on the bulk linear magnetoelectric coefficient and allow firm electrical control of spin manipulation in a graphene channel. When combined with the good dielectric properties of Cr_2O_3, including high relative permittivity (~11–13) [26], high breakdown field [10, 15] and low leakage current [27], the magnetoelectric properties we have observed show that exchange-based spin FET's on graphene are likely to succeed with this material as a gate. Other magnetoelectric and multiferroic oxides may also be considered in graphene spin-FETs, especially including the ferrites, which have unique higher order magnetoelectric coupling effects [28]. However, chromia is a simple target for initial device demonstrations.

5 Conclusion In summary, we report the creation of magnetoelectric Cr_2O_3 films on graphite and graphene on SiC at relatively low substrate temperatures. These films are shown to be magnetoelectric by imaging spontaneous magnetic and electric domains after magnetoelectric annealing. In addition, local electric fields applied with a biased AFM tip can be used to "write" arbitrary patterns that appear in both electrostatic and magnetic force microscopy images. These films are compatible with a variety of device structures including traditional three terminal spin-FETs [6] and nonlocal spin valves [1]. The magnetoelectric functionality we report here is the crucial missing piece in realizing the long-standing challenge of spin manipulation using exchange interactions at an oxide-graphene interface.

Supporting Information Additional supporting information may be found in the online version of this article at the publisher's website.

Acknowledgements We acknowledge useful discussions and technical assistance of Professor J. P. Maria. This work was supported by the Army Research Office under contract number W911NF-04-D-0003.

References

[1] W. Han, R. K. Kawakami, M. Gmitra, and J. Fabian, Nature Nanotechnology **9**(10), 794–807 (2014).
[2] I. Appelbaum, B. Q. Huang, and D. J. Monsma, Nature **447**(7142), 295–298 (2007).
[3] S. Datta and B. Das, Appl. Phys. Lett. **56**(7), 665–667 (1990).
[4] A. Avsar, J. Y. Tan, T. Taychatanapat, J. Balakrishnan, G. K. W. Koon, Y. Yeo, J. Lahiri, A. Carvalho, A. S. Rodin, E. C. T. O'Farrell, G. Eda, A. H. C. Neto, and B. Ozyilmaz, Nature Commun. **5**, 4875 (2014).
[5] H. Haugen, D. Huertas-Hernando, and A. Brataas, Phys. Rev. B **77**(11), 115406 (2008).
[6] Y. G. Semenov, K. W. Kim, and J. M. Zavada, Appl. Phys. Lett. **91**(15), 153105 (2007).
[7] M. Fiebig, J. Phys. D: Appl. Phys. **38**(8), R123–R152 (2005).
[8] J. A. Kelber, C. Binek, P. A. Bowden, and K. Belashchenko, Patent No. US20140231888 A1 (2014).
[9] A. Iyama and T. Kimura, Phys. Rev. B **87**(18), 180408 (2013).
[10] X. He, Y. Wang, N. Wu, A. N. Caruso, E. Vescovo, K. D. Belashchenko, P. A. Dowben, and C. Binek, Nature Mater. **9**(7), 579–585 (2010).
[11] T. Ashida, M. Oida, N. Shimomura, T. Nozaki, T. Shibata, and M. Sahashi, Appl. Phys. Lett. **104**(15), 152409 (2014).
[12] T. Ashida, M. Oida, N. Shimomura, T. Nozaki, T. Shibata, and M. Sahashi, Appl. Phys. Lett. **106**(13), 132407 (2015).

[13] S. Cao, X. Zhang, N. Wu, A. T. N'Diaye, G. Chen, A. K. Schmid, X. M. Chen, W. Echtenkamp, A. Enders, C. Binek, and P. A. Dowben, New J. Phys. **16**, 073021 (2014).
[14] W. Echtenkamp and C. Binek, Phys. Rev. Lett. **111**(18), 187204 (2013).
[15] K. Toyoki, Y. Shiratsuchi, A. Kobane, S. Harimoto, S. Onoue, H. Nomura, and R. Nakatani, J. Appl. Phys. **117**(17), 17d902 (2015).
[16] K. Toyoki, Y. Shiratsuchi, A. Kobane, C. Mitsumata, Y. Kotani, T. Nakamura, and R. Nakatani, Appl. Phys. Lett. **106**(16), 162404 (2015).
[17] K. D. Belashchenko, Phys. Rev. Lett. **105**(14), 147204 (2010).
[18] A. G. Swartz, P. M. Odenthal, Y. F. Hao, R. S. Ruoff, and R. K. Kawakami, ACS Nano **6**(11), 10063–10069 (2012).
[19] X. M. Chen, H. Kazi, Y. Cao, B. Dong, F. L. Pasquale, J. A. C. Santana, S. Cao, M. Street, R. Welch, C. Binek, A. Enders, J. A. Kelber, and P. A. Dowben, Mater. Chem. Phys. **149**, 113–123 (2015).
[20] A. Sandin, A. Pronschinske, J. E. Rowe, and D. B. Dougherty, Appl. Phys. Lett. **97**(11), 113104 (2010).
[21] M. C. Biesinger, C. Brown, J. R. Mycroft, R. D. Davidson, and N. S. McIntyre, Surf. Interf. Anal. **36**(12), 1550–1563 (2004).
[22] L. H. Li and Y. Chen, J. Appl. Phys. **116**(21), 213904 (2014).
[23] C. Cen, S. Thiel, G. Hammerl, C. W. Schneider, K. E. Andersen, C. S. Hellberg, J. Mannhart, and J. Levy, Nature Mater. **7**(4), 298–302 (2008).
[24] H. Kinoshita, M. Umeno, M. Tagawa, and N. Ohmae, Surf. Sci. **440**(1–2), 49–59 (1999).
[25] H. X. Yang, A. Hallal, D. Terrade, X. Waintal, S. Roche, and M. Chshiev, Phys. Rev. Lett. **110**(4), 046603 (2013).
[26] P. H. Fang and W. S. Brower, Phys. Rev. **129**(4), 1561–1561 (1963).
[27] S. H. Lim, M. Murakami, S. E. Lofland, A. J. Zambano, L. G. Salamanca–Riba, and I. Takeuchi, J. Magn. Magn. Mater. **321**(13), 1955–1958 (2009).
[28] G. Catalan and J. F. Scott, Adv. Mater. **21**(24), 2463–2485 (2009).